

Terahertz Heterodyne Array Receivers for Astronomy

Urs U. Graf¹ · Cornelia E. Honingh¹ · Karl Jacobs¹ ·
Jürgen Stutzki¹

Received: 1 February 2015 / Accepted: 11 May 2015 /
Published online: 16 June 2015
© Springer Science+Business Media New York 2015

Abstract We review the development of multi-pixel heterodyne receivers for astronomical research in the submillimeter and terahertz spectral domains. We shortly address the historical development, highlighting a few pioneering instruments. A discussion of the design concepts is followed by a presentation of the technologies employed in the various receiver subsystems and of the approaches taken to optimize these for current and future instruments.

Keywords Radio astronomy · Terahertz receiver · Heterodyne array

1 Introduction

Heterodyne spectrometers are very powerful instruments to study the physics of the atomic and molecular gas in space. With their high spectral resolving power of $R > 10^6$, they are the only instruments capable of resolving the velocity structure

✉ Urs U. Graf
Graf@ph1.uni-koeln.de

Cornelia E. Honingh
Honinzh@ph1.uni-koeln.de

Karl Jacobs
Jacobs@ph1.uni-koeln.de

Jürgen Stutzki
Stutzki@ph1.uni-koeln.de

¹ I. Physikalisches Institut, Universität zu Köln Zùlpicher Straße 77, 50937 Köln, Germany

of spectral lines even from cold and quiescent interstellar gas. Beyond identifying species and measuring their abundance, this allows studying the gas dynamics through the Doppler shift of the line emission. In many cases, only high resolution spectroscopy provides the means to assign the emission to the proper source component, which is the basis to derive physical quantities like temperature and densities through an excitation analysis.

Over the past decades, these instruments have become ever more sensitive and have pushed radio detection techniques to ever higher frequencies. Although low-noise amplifiers for frequencies close to 1 THz [1, 2] are being developed, essentially all heterodyne receivers beyond approximately 100 GHz still have to use a low-noise mixer for downconversion to frequencies around 1–10 GHz before the first amplification stage.

With the introduction of superconductive detectors [3], the sensitivity is now rapidly approaching the fundamental physical limit for coherent detection of $T_{RX,SSB} \geq h\nu/k_B$ [4]. Near quantum limited detection is state of the art through most of the submillimeter wavelength range (0.3 – 1 THz), where superconductor-isolator-superconductor (SIS) devices are the mixers of choice. Beyond the operation limit of SIS mixers around 1.2 THz, the highest sensitivity is obtained with superconductive hot electron bolometers (HEB) (Section 4.2). Figure 1 gives an overview of state-of-the-art sensitivities, as obtained with the ALMA receivers and with GREAT on SOFIA.

A significant further increase of the receiver’s productivity is, therefore, only possible by increasing the number of independent detector channels. This can be achieved in the spectral domain by increasing the instantaneous bandwidth of the

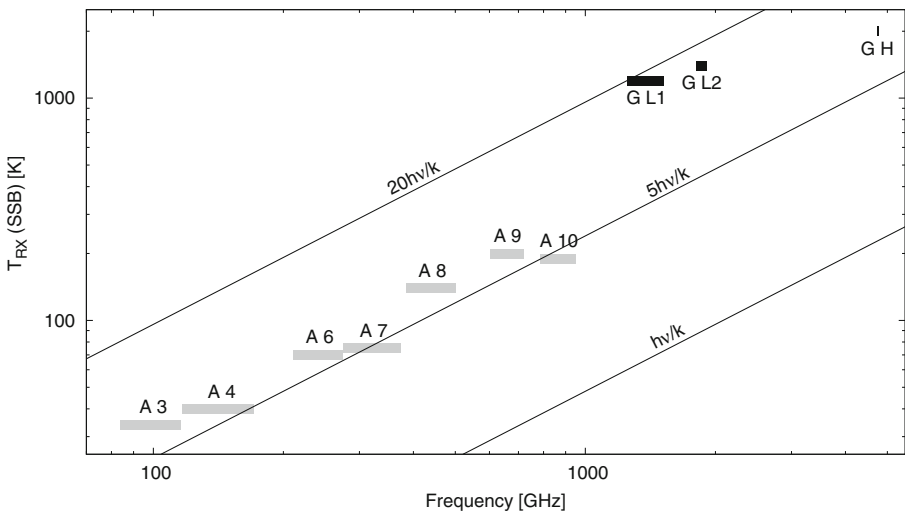


Fig. 1 State-of-the-art performance of astronomical receivers in the submillimeter and low THz regime as demonstrated by the ALMA [5] receivers using SIS mixers (grey) [6–12] and by GREAT [13, 14] using HEBs (black). The straight lines indicate the quantum limit $h\nu/k_B$ and multiples of it

instrument, or, if the emphasis is on observations of extended sources, by adding more detector pixels to increase the receiver's mapping speed.

Owing to their complexity, however, submillimeter and terahertz heterodyne receivers are mostly built as single pixel instruments. A high per-pixel effort is necessary to pass the downconverted signal at the intermediate frequency (IF) through low-noise high frequency amplification and possibly further processing, before analyzing it in a spectrometer backend (Section 4.4).

Only during the last 15 years, the first submillimeter array receivers have been deployed to astronomical telescopes [15–20]. These first generation instruments have a modest number of pixels, between 10 and 20. Recently, the first array with more than 50 pixels went into operation [21] (Fig. 2).

While submillimeter receivers can be operated from several ground-based telescope sites, the opacity of the earth's atmosphere in the far infrared wavelength domain restricts terahertz instruments to operation from platforms above the atmosphere, like satellites or balloon- or aircraft-borne telescopes. After the end of the Herschel [22] and STO [23] missions, SOFIA [24] is currently the only operational observatory for this spectral regime and the GREAT instrument [25] is, at present, the only heterodyne spectrometer available in the far infrared.

This scarceness of observing opportunities—both in the submillimeter and terahertz regime—together with the high operating cost of the observatories, makes it imperative to maximize the data output of the receivers, which, in turn, implies the need for multi-pixel receivers. In the near future, we expect to see moderate size

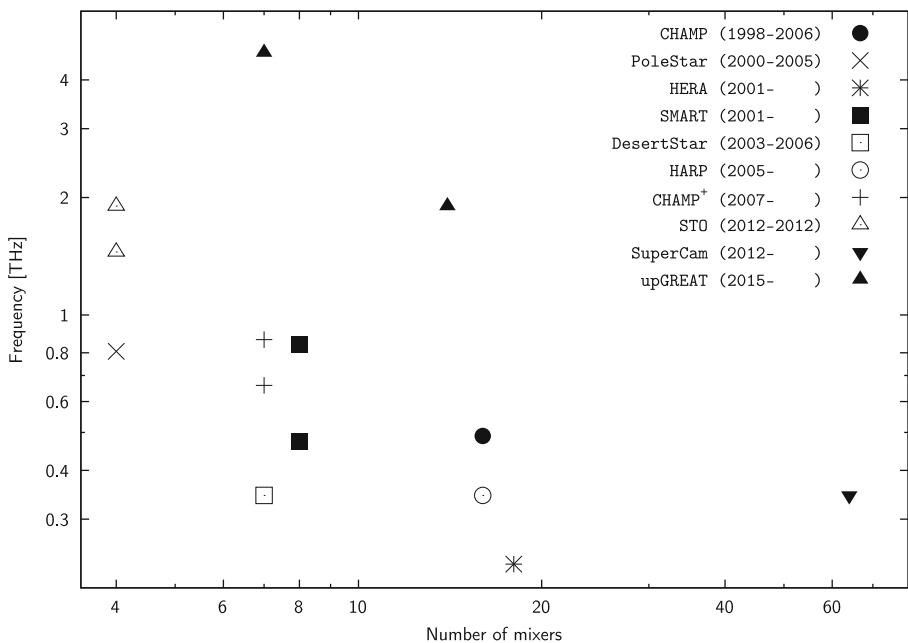


Fig. 2 Pixel count and operating frequency of heterodyne receivers above 200 GHz. The approximate period of activity is also given

arrays for terahertz frequencies, and an increasing number of arrays with on the order of 100 pixels in the submillimeter.

In the following, we will review the development of astronomical heterodyne array receivers for frequencies beyond approximately 0.3 THz. We will discuss the specific needs that drive the design of these instruments, ways how these needs can be satisfied, and the compromises that may have to be made on the path to a working instrument.

2 History

The first heterodyne array for wavelengths of $\lesssim 1$ mm was an 8 pixel cooled Schottky mixer array for the NRAO 12 m antenna on Kitt Peak, Arizona [26]. With the turn of the century the first SIS arrays were installed, which quickly moved up to higher observing frequencies. We will shortly review the design features of some of these pioneering instruments¹.

CHAMP/CHAMP⁺ CHAMP [15] was a 4×4 pixel array for the $625 \mu\text{m}$ atmospheric window first installed at the Caltech Submillimeter Observatory [28] on Mauna Kea, Hawaii in 1999. The array was composed of two polarization split interleaving subarrays of 8 pixels each, which reduced the beam spacing by a factor of $\sqrt{2}$. The whole optics setup of CHAMP, including four Martin–Puplett interferometers for LO-diplexing and single sideband filtering, was cooled to ≈ 15 K to decrease thermal background. Image derotation was achieved by rotating the receiver cryostat. In 2007, CHAMP, now operating at APEX [29], was upgraded to CHAMP⁺ [19] to cover the 660 GHz and the 850 GHz atmospheric windows in two subarrays of 7 pixels each, while maintaining the basic optomechanical design. Later, the original autocorrelator backend was replaced by digital Fourier transform spectrometers (DFTS).

HERA HERA [30] is a 3×3 pixel array for 215–270 GHz installed in 2001 at the IRAM 30 m telescope [31] on Pico Veleta/Spain. Each pixel is covered by two mixers, one for each polarization. The detectors are tunable single sideband SIS mixers. Waveguide splitters distribute the local oscillator signals. Autocorrelators and filterbanks are used as spectrometer backends. HERA was the first heterodyne array to use a K-mirror image rotator to compensate optical field rotation.

SMART SMART [16] has a 2×4 pixel footprint, which is covered simultaneously in two polarization split wavelengths bands: 460–490 GHz and 800–880 GHz. It was installed on the KOSMA 3 m telescope [32] on Gornergrat/Switzerland in 2001 and transferred to the NANTEN2 telescope [33] on Pampa la Bola/Chile in 2008. SMART uses single-ended SIS mixers with diplexer coupled local oscillators.

¹More detail can be found in [27]

Acousto-optical spectrometers (AOSs) were initially used as backends, but recently replaced by DFTSs. SMART pioneered the use of Fourier gratings to distribute the LO power to the array pixels. Image derotation is achieved with a K-mirror type image rotator.

HARP HARP [20] is a 4×4 element array for 325–375 GHz, installed at the James Clerk Maxwell Telescope [34] on Mauna Kea/Hawaii in 2005. HARP uses an interferometer for single-sideband filtering. The local oscillator signal is meandering along mixers through 16 beam splitters, which extract small amounts of the LO power and feed it to the mixers.

SuperCam SuperCam [21] is the first submillimeter array to cross the 50 pixel boundary. It is an 8×8 pixel array, which is approaching standard operation at the Heinrich Hertz Telescope [35] on Mount Graham/Arizona. Instead of using individual mixer blocks, the focal plane is composed of eight monolithic rows, each containing eight mixers. The LO is split into an 8×8 array by waveguide splitters and is then optically coupled to the mixers with a Mylar beamsplitter. DFTS are used as spectrometer backends.

Terahertz Arrays Until now, all heterodyne arrays still operate at frequencies below 1 THz. A first attempt at a 2×2 pixel, balloon-borne dual frequency array (STO [23]) was only short lived, but will see a continuation in the upcoming STO-2 mission. The modular GREAT instrument [25] is currently being upgraded to become upGREAT [36], which accommodates two array receiver bands: a polarization split 2×7 pixel "low frequency" array around 1900 GHz and a 7 pixel high frequency array at 4700 GHz. Commissioning of upGREAT on SOFIA will start in 2015.

3 Array Receiver Requirements and Constraints

The dominating requirement of an astronomical receiver is sensitivity. The observing time needed to reach a given signal-to-noise level on a weak signal is proportional to the square of the receiver noise temperature, the conventional measure of receiver sensitivity. The important consequence of this almost trivial statement is that an increase in pixel count can usually not make up for sub-standard performance of the array elements. Each pixel in an array receiver should have essentially the same sensitivity as a good single pixel receiver to take the full multiplexing advantage of the array and to justify the effort of building such a complex machine [37].

This requirement not only calls for the best possible mixers but also for a low-loss signal path from the detectors to the telescope. If the array uses additional optical elements compared to a single pixel receiver, these elements are not allowed to contribute significantly to the noise budget.

Similarly, the stability of an array receiver should not be worse than the stability of a single pixel instrument. Allen variance [38] minimum times² should be several tens of seconds or more to allow using efficient observing modes like *on-the-fly* scanning of a source.

With increasing pixel count, the receiver becomes a spectroscopic *camera*. In contrast to regular cameras, however, a heterodyne receiver does not produce a fully sampled³ picture of the source. Since the receiver is detector noise limited, it is important to design for optimum single mode optical coupling to the telescope to achieve best possible sensitivity. This is only possible, if a pixel spacing of at least two resolution elements is chosen (Section 4.1).

To fully sample a source, the gaps between pixels have to be filled in by multiple observations at slightly shifted array pointings. Often, it is most efficient to do this in an *on-the-fly* scanning mode with continuous data acquisition.

The complexity of an array receiver scales almost linearly with the pixel count. Only the local oscillator, the cryogenic, and most of the optomechanical subsystems of the instrument can be shared by all receiver channels. A considerable fraction of the receiver complexity is located in the signal path from the mixer to the spectroscopic backend and has to be implemented separately for each pixel. To make a large array project manageable, the complexity of each receiver channel, therefore, has to be reduced as far as possible. New developments of, e.g., integrated mixer focal planes [39] (Section 4.2) work in this direction, but so far all operational array instruments are still basically an assembly of many individual receiver channels.

Individual manual tuning of each mixer is prohibitively slow for a large array. Most tuning tasks have to be automated for efficient operation of the system. Thus, the instrument needs to be fully computer controllable with fast and reliable algorithms to monitor the receiver status and to optimize the operating parameters.

4 Instrument Design

4.1 Optics

Designing optics for an array receiver is most easily done in a hybrid way: the Gaussian optics formalism traces the evolution of a single beam through the setup, and geometrical optics describes how the beam axes of the array pixels propagate through the system. In a conservative design with large F -numbers and small incidence angles on active mirrors, this approach generally yields a good description of the optical properties. Physical optics simulation programs⁴ can be used to refine the results.

²Allen variance minimum time is a measure for the stability of a receiver. It sets the maximum time the receiver can integrate before signal fluctuations are dominated by receiver drifts.

³as defined by the Rayleigh criterion: pixel spacing equal to one half of the size of a resolution element

⁴e.g., GRASP by TICRA, Copenhagen, Denmark

As in a single pixel receiver, the purpose of the optics is to match the beam of the mixer feed to the telescope. Since heterodyne receivers are detector noise limited, a good optical coupling to the telescope is essential for the receiver performance.

The total optical magnification M , is then given as the ratio of the telescope focal plane beam waist w_{FP} to the mixer beam waist w_M

$$M = \frac{w_{FP}}{w_M} = \frac{0.216 \cdot \sqrt{T_E} \cdot F \cdot \lambda}{w_M}, \quad (1)$$

where we expressed w_{FP} by the illumination edge taper T_E and the telescope focal ratio $F = f/D$ [40]. Assuming a typical edge taper of 14 and a mixer feed horn beam waist of 1.8 wavelengths [41, 42] the required magnification is about $0.5 \cdot F$, which amounts to 5 to 10 on most telescopes.

In a focal plane array, an additional optical constraint arises: the array of mixer feeds needs to be matched to the focal plane of the telescope. If the mixers are arranged in a planar array with parallel beam axes, the mixer plane has to be at a geometrical image of the telescope focal plane, such that the mixer beams get imaged into parallel beams in the telescope focal plane⁵. Both the waist sizes and the spacing between the beams then scale by the same magnification M (see Appendix):

$$s_{FP} = M \cdot s_M \quad \text{and} \quad w_{FP} = M \cdot w_M. \quad (2)$$

Thus, the ratio of the mixer spacing s_M to the mixer beam waist w_M directly sets the spacing $\Delta\theta$ of the array beams on the sky. Using Eqs. 1 and 2, we obtain:

$$\frac{\Delta\theta}{\Theta_{FWHM}} = \frac{s_{FP}/f}{1.2 \cdot \lambda/D} = \frac{s_{FP} \cdot 0.216 \cdot \sqrt{T_E}}{1.2 \cdot w_{FP}} = 0.18 \cdot \sqrt{T_E} \cdot \frac{s_M}{w_M}, \quad (3)$$

where we assume a FWHM beam width Θ_{FWHM} on the sky of $1.2 \cdot \lambda/D$.

In order to obtain a conveniently small spacing of the array beams on the sky it is, therefore, imperative to minimize the spacing between the mixers and to maximize the mixer beam waists for a given mixer pitch. However, since each pixel's aperture size is limited to the size of the mixers, the ratio s/w cannot be arbitrarily small. Diffraction losses start to become significant for values of $s/w < 3$ (Appendix), which according to Eq. 3 limits the beam spacing on the sky to $\Delta\theta > 2 \cdot \Theta_{FWHM}$.

In a classical heterodyne array with individual mixers, the typical size of one pixel is on the order of 10 mm, and thus requires a beam waist of $w_M \gtrsim 3$ mm, which is much larger than the waist produced by a conventional feed horn in the terahertz regime. At frequencies up to a few hundred gigahertz, it is possible to design horns with ultra-large waists [43], which may be suited for array applications. At even higher frequencies, each mixer requires an individual optical element to collimate its beam, before it is injected into the common array optics. This can be achieved by a simple lens (e.g., [15]) or with a fully reflective design like the CHARM [44] setup.

Although any optical system fulfilling the imaging condition can be used, it is often convenient to compose the optics of one or more Gaussian telescopes (GT, Fig. 3), where two optical elements are placed at a distance equal to the sum F of

⁵ A slight additional tilt of the beams in the focal plane may be chosen to improve coupling to the telescope.

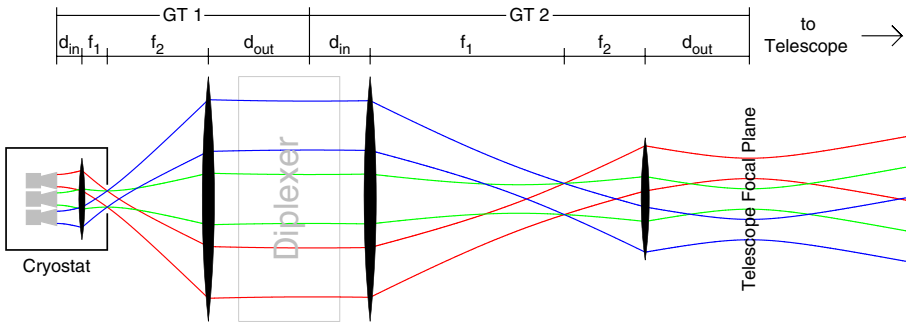


Fig. 3 Schematic beam path in a typical array optics setup using two Gaussian telescopes (GT) for reimaging. GT 1 creates a large image of the mixer focal plane, where for example an LO diplexer could be located. GT 2 demagnifies to match the telescope focal plane. The cryostat window is located at an image of the telescope aperture, where the total beam cross section is minimal. For compactness and clarity, the imaging elements are drawn as lenses, although mirrors are more commonly used in real instruments

their focal lengths: $F = f_1 + f_2$. The magnification of such an arrangement is then given by the ratio of the two focal lengths: $M_{GT} = w_{out}/w_{in} = f_2/f_1$, and the waist locations d_{in} and d_{out} obey the relation

$$d_{out} = MF - M^2d_{in}. \tag{4}$$

If an intermediate image of the focal plane is needed, for instance to accommodate a local oscillator diplexer (Section 4.3.2), two GTs may be used, where one GT reimages the telescope focal plane to the diplexer plane, and a second GT reimages the diplexer plane to the mixer plane.

A particularly interesting case of Eq. 4 is $d_{in} = f_1$, which implies $d_{out} = f_2$ (GT 1 in Fig. 3). If $d_{in} = f_1$ is chosen, we get an image of the aperture plane between the two optical elements. Here, the beam waists of all pixels are at the point where all array beams intersect, which reduces the cross section of the total light path to the beam waist size of a single beam, creating a very attractive location to place the cryostat’s vacuum window.

4.1.1 Cryostat Window

The window itself is a critical element in the beam path. It needs to be strong enough to support the external air pressure, and at the same time, it has to be transparent enough to not adversely affect the receiver sensitivity.

The simplest window design is a plane parallel dielectric window with a thickness matched to place a Fabry–Perot transmission fringe on the receiver’s measurement frequency. This is usually a good choice, if the window is small, the receiver’s frequency coverage is moderate, and the wavelength is relatively long. For instance, the SMART receiver [16] uses a 0.9-mm-thick PTFE window to match its two frequency bands (470 and 810 GHz) in 4th and 7th Fabry–Perot transmission orders, respectively.

With increasing window thickness or increasing frequency, the absorption losses become more severe and at the same time the fringes become more narrow to the point that window losses, particularly at the band edges, become undesirably high. Therefore, for larger windows or at higher frequencies, anti-reflection (AR) coated windows made from low-loss crystalline solids are generally preferable. The window material of choice in the terahertz regime is high-resistivity silicon. Due to its high refractive index ($n \approx 3.5$), silicon requires an AR treatment, which may be obtained by applying a coating of parylene ($n \approx 1.6$) [45].

A more optimized AR treatment can be created by modifying the effective refractive index in the surface layer by sub-wavelength structuring of the material. Such an artificial dielectric layer can be tailored precisely to the needs. The structure can be manufactured either by etching a pattern into the silicon surface or by cutting grooves into it with a dicing saw. Both processes have been shown to produce the expected results [46, 47].

4.1.2 Optics Manufacturing and Alignment

A significant fraction of the array optics may be at cryogenic temperatures. To minimize the thermal emission of optical elements, it may even be chosen to place essentially all the optics inside the cryostat. Optical alignment of such a setup is difficult, because the alignment elements either need cryogenic mechanisms or are not accessible while the instrument is operational. This situation is worsened by the fact that many terahertz optics components (e.g., polarizer grids) are not suitable for alignment with a visible laser beam.

These difficulties can be turned into an advantage by using modern CAD/CAM techniques. With ultra-precision milling machines surface accuracies and roughnesses down to below 1 micron can be achieved by direct milling. One micron corresponds to $\lambda/50$ at 6 THz and is, therefore, more than sufficient for optical surfaces in the submillimeter and well into the terahertz range [48].

Thus, using a standard CAD program, the optics can be modeled as one or a few monolithic components, each containing a possibly large number of optical surfaces together with all mounting references needed to assemble the component into the complete optics unit. Using 5-axes milling techniques, such components, which may be rather complex, can then be cut from a single block.

The advantage of this monolithic optics approach is that the need for optical alignment is almost completely avoided, since all surfaces are either directly cut or defined by their mounting surfaces into the position where they need to be with an intrinsic accuracy given by the milling machine. The method is particularly powerful for reflective optics where the beams are imaged by mirrors instead of lenses. For instance, the optics unit of STO [49] contains 12 active mirrors cut into a single block of aluminum (Fig. 4).

Modern CAD programs provide interfaces to implement Gaussian optics design formulae within the CAD environment. Thus, the input data for the *mechanical* design may be *optical* parameters, which then directly define the shape of the surfaces to be cut. Together with an integrated CAM process, this yields a very simple and reliable way of creating even complex optical systems.

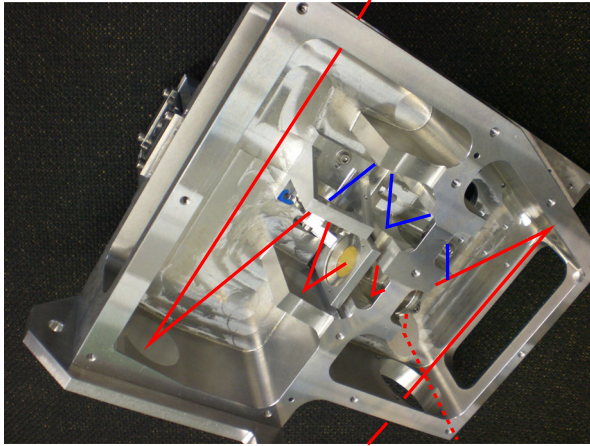


Fig. 4 Partly assembled main optics unit of STO, which contains 12 imaging mirrors machined monolithically from a single block of aluminum. The *colored lines* give a simplified indication of the beam path through the unit

For cryogenic optics, the thermal shrinkage of the material may be significant. Between room temperature and 4 K, aluminum shrinks approximately by 4 %, which may create a relevant change in the optical behavior of the setup. This can be taken care of by defining an artificial length unit in the CAD program, that is 4 % longer than the normal unit. The part is then manufactured accordingly larger and shrinks into dimension upon cooling.

4.1.3 Sampling Strategies and Image Rotation

We have seen above that heterodyne arrays have to undersample the focal plane in order to optimize their sensitivity. Thus, to get a fully sampled map of an extended astronomical object, the source has to be measured at a number of different pointings to fill in the gaps between the array beams. For instance, if the array beam spacing corresponds to 2.5 times the beam FWHM, $5 \times 5 = 25$ pointings are required to get a Nyquist sampled⁶ image.

The optimum sampling strategy depends on a number of factors like the agility of the telescope, the required integration times, the stability time scale of the receiver, and the size of the source relative to the field of view (FOV) of the array.

For extended sources, it is usually most efficient to scan the object in an *on-the-fly* pattern, where samples are measured at high rates, while the telescope is continuously slewing across the source. If the scanning direction is chosen at an oblique angle with respect to the array orientation, it may be possible to obtain full sampling along a strip of width equal to the FOV of the array. On a large source, the unavoidable fringing effects occurring at the ends of the strips can be tolerated.

⁶Spacing equal to FWHM / 2

If the array pixels are arranged in a hexagonal grid, the areal sampling density is $\sim 15\%$ higher compared to a more conventional rectangular array, and, accordingly, less pointings are needed to create a fully sampled image. On the other hand, it is more difficult to obtain a constant sampling density over a large area, and fringing effects are slightly more severe with a hexagonal array.

An additional point that affects the sampling strategy is image rotation. For mechanical reasons, almost all submillimeter and terahertz telescopes use an azimuth-elevation mount. This leads to a rotation of the image in the focal plane while a source is being tracked by the telescope. This rotation makes it virtually impossible to obtain a homogeneously and fully sampled image of an extended source.

Image rotation can be compensated by optomechanical means. For example, SMART uses a K-mirror type image rotator, CHAMP⁺ rotates the receiver cryostat to follow the image, and the SOFIA telescope has the ability to rotate, within limits, around the line of sight and can compensate image rotation for short integrations.

To avoid the additional mechanical complexity of image derotation, somewhat inhomogeneous sampling densities are often accepted and elaborate scanning patterns are being developed to minimize them [50, 51].

4.2 Detectors

The noise performance and conversion efficiency of the frequency mixer, as the first element in the signal chain, determines the system performance. Schottky diode mixers have been used in earlier astronomical receivers but are impractical for modern arrays due to their limited sensitivity and their high local oscillator power requirement in the $100\ \mu\text{W}$ range per pixel. The extreme sensitivity needed for radio astronomy and the low available local oscillator power in the submillimeter and terahertz range demand using superconducting devices as mixers. Below approximately 1 THz SIS junctions are the detectors of choice, and at higher frequencies, hot electron bolometer (HEB) mixers are used.

As these detectors are very small in comparison to the operating wavelength, they need antennas to couple to free-space radiation. This can either be accomplished with planar antennas or by coupling probes to waveguides with a subsequent waveguide horn.

At submillimeter wavelengths, planar antennas have to be immersed into a dielectric halfspace to avoid dielectric surface modes. The result is a substrate-lens antenna mixer, often called a quasioptical mixer [52]. The technology is simple because thick substrates can be used, but the beam quality can be a challenge. As the lens usually has an F -number around 1, small offsets of the planar antenna from the focus point can result in substantial beam squint which is a problem for arrays.

Waveguide mixers use horn antennas, which decouple the optics parameters from the detector circuit. A disadvantage is the requirement of very thin substrates to avoid substrate surface wave losses. This can be overcome by using extremely thin silicon substrates using silicon-on-insulator (SOI) techniques. This approach has several advantages over the quartz substrates used in earlier mixer generations. Silicon micromachining allows producing arbitrary substrate shapes and beam lead

contacts can be used [14, 53]. This is favorable for the assembly of arrays of detectors, at least as long as arrays are still made from multiplication of single detectors. Moreover, on silicon, it is possible to integrate complex circuitry together with the mixer.

An example is the integration of two mixers with a 180 degree on-chip hybrid coupler forming a balanced mixer [53] (Fig. 5). A balanced mixer provides a separate local oscillator port, eliminating the need for a diplexer for signal and LO and thus using the full available LO power. In addition, any LO amplitude noise, which can be considerable (Section 4.3.1), is suppressed [54]. Integrating the hybrid coupler on-chip is very attractive for array applications as it results in a very small mixer footprint compared to the more conventional waveguide hybrid solution [55].

Sideband separating designs [8, 9] use two mixers combined to provide two separate output ports for the upper and lower signal sideband. This makes it easier to disentangle emission from the two sidebands in a crowded spectrum and also avoids noise contamination by atmospheric absorption features in the image sideband of the observed signal.

The next development step then is the combination of the two techniques to form a balanced sideband separating mixer involving four mixers.

An important requirement for detectors in an array receiver is the detector volume. Once the detector footprint is larger than about $10 \times 10 \text{ mm}^2$, the detector size starts to drive the cryostat dimension. Implementing these advanced mixer designs on-chip in a small mixer block is, therefore, crucial to using them in a focal plane array.

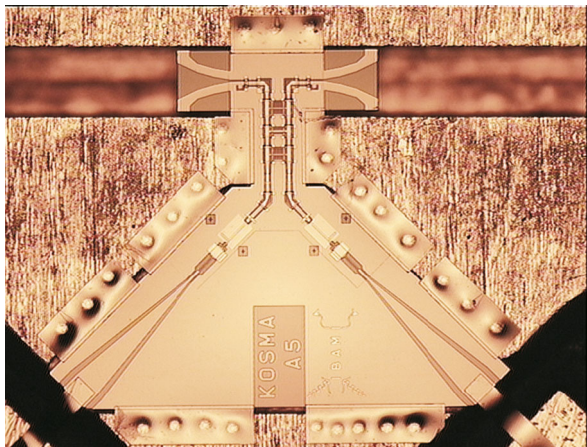


Fig. 5 460 GHz balanced SIS mixer RF-chip on a $9 \mu\text{m}$ thick shaped silicon substrate. The 2 antennas pick up the LO and the signal from the waveguides and lead them to the 90 degree hybrid on the same substrate. The SIS mixers are in the 2 side arms after the hybrid on the white SiO_2 patch. The chip is mounted into the waveguide block with beam leads. The 2 IF contact leads can just be seen in the lower corners of the picture. The physical width of the area depicted is about 1.5 mm

For large arrays ($\gtrsim 100$ pixels), the approach of stacking an array of single-pixel mixers together will reach its limits. There are suggestions to more advanced concepts using silicon micromachined waveguides with stacked layers of silicon circuits [39].

4.2.1 Superconductor-Insulator-Superconductor Devices

The sensitivity of SIS tunnel junctions used as mixers stems from the extremely nonlinear voltage dependence of the tunnel current, caused by the singularity of the density of states of the quasiparticles in the superconducting electrodes. The output shot noise of SIS mixers with good quality tunnel barriers is extremely low.

At submillimeter frequencies where the voltage width of the IV-curve nonlinearity is smaller than the voltage scale of the radiation frequency $h\nu/e$ (h : Planck's constant, ν : frequency, e : electron charge), the SIS mixer behaves as a quantum mixer, as described in [56], which gives a complete theoretical description of the mixer functionality. The required local oscillator power at submillimeter frequencies is in the $1 \mu\text{W}$ range, scaling with the square of the frequency. The gap energy of the superconducting electrodes, which is proportional to their critical temperature, limits SIS mixers to frequencies lower than the sum of the gap frequencies of the two electrode materials.

Even if typical sizes of SIS tunnel junctions are in the $1 \mu\text{m}^2$ range, their relatively large geometrical capacitance, which tends to short out the RF currents, makes RF matching to waveguides or antennas challenging. A breakthrough was achieved when superconducting circuits were integrated with the tunneling junctions, resulting in broadband, high- Q matching circuits that made it possible to exploit the intrinsic quantum limited sensitivities in practical mixers [57–59].

The superconductivity of the tuning circuit is also limited by its gap frequency, which is around 700 GHz for Niobium. SIS mixer tuning circuits above this frequency use a combination of higher gap superconducting materials like NbTiN and normal conducting metals like gold or aluminum [60, 61]. Up to 700 GHz SIS mixers reach quantum limited sensitivity. Above 700 GHz, the receiver noise increases due to ohmic losses in the integrated tuning circuit, but stays in general below five times the quantum limit.

SIS tunnel junction mixers need a magnetic field of several hundred Gauss to suppress the unwanted Josephson effect caused by Cooper pair tunneling. Conventionally, this is done with superconducting electromagnets. For arrays, this is cumbersome both in terms of volume and wire count. A feasible alternative is the use of tiny permanent magnets close to the tunnel junctions, where again the arbitrarily shapable Silicon substrates are advantageous, if several SIS junctions need separate magnets. The close proximity of the magnets to the junction helps to reduce magnetic crosstalk between adjacent mixers.

4.2.2 Hot Electron Bolometers

Due to their intrinsic frequency limit, SIS mixers have not seen application beyond about 1.2 THz. At higher frequencies, the most sensitive heterodyne detectors are

superconducting hot electron bolometers [62, 63]. They consist of a superconducting film of a few nanometer thickness and a few 100 nm length. With the width of the device determined by the required matching impedance and the surface resistance of the film, this creates a very small detector volume, for example, $L \times W \times d = 0.2 \times 2 \times 0.004 \mu\text{m}^3$, and a corresponding low local oscillator power requirement. The bolometer time constants are in the picosecond range, so that they can be used for frequency mixing up to a few gigahertz of intermediate frequency. This time constant depends among other factors on the substrate of the HEB, since the main cooling path of the thermalized electrons is via the electron phonon interaction and the phonon escape time.

As absorbers for the photon energy, they do not have a practical RF frequency limit and they act largely as a resistive element to the incoming radiation. Contrary to SIS mixers, no high- Q matching circuit is needed. Advantages are the rather low local oscillator requirement (50–300 nW at the device) and no need for a magnetic field. A downside is the roll-off at the intermediate frequency (3–4 GHz in present practical mixers, set by the thermal time constant), although there are promising developments with MgB_2 HEBs showing the feasibility of an IF roll-off frequency around 10 GHz [64, 65]. Also, HEB mixers are sensitive to LO power fluctuations, resulting in IF power instability. A full theoretical description of the HEB mixer that could give guidelines to optimize its performance is still missing.

Double sideband noise temperatures of practical mixers are in the 500–1000 K range from 1 to 5.3 THz, reaching below 10 times the quantum limit. Most earlier mixer results were published for substrate-lens quasi-optical mixers [66–68]. Waveguide mixers have also been developed [69, 70] and recently have successfully collected astronomical data with state-of-the-art sensitivity in the GREAT receiver on SOFIA [13, 14] (Figs. 1, 6).

4.2.3 Horn Antennas

The feed horn couples the free space radiation into the detector waveguide. Several classical horn designs are commonly used, e.g., corrugated [71, 72], dual mode [42], or diagonal horns [73]. In general, the horns with the best coupling to a fundamental Gaussian beam mode (*Gaussicity*) are the most difficult and expensive to manufacture. This is particularly true for corrugated feed horns, which are usually manufactured by electroforming from complex profiled mandrels.

Although corrugated feed horns for low terahertz frequencies can be manufactured [74], it would be very cumbersome to produce many units for an array application. With the advent of powerful computers and modeling algorithms, it has become possible to numerically design horns that have similarly good properties as corrugated feeds, but use a much smoother wall surface [75], and, therefore, are much easier to manufacture.

Novel manufacturing techniques have been proposed to avoid the slow process of electroforming horn antennas. In the platelet horn [76], the horn is built by etching apertures into thin sheets of metal or silicon and then stacking them to form a layered horn antenna. Depending on the variation of aperture size within the stack, arbitrary

horn profiles can be approximated to within the thickness of individual layers. Since each sheet may have a whole array of apertures, this approach is well suited for horn arrays. Limitations at high frequencies are the demanding manufacturing tolerances and the difficulties of bonding the sheets together. In particular, the layers near the horn aperture—to minimize the horn spacing (see Section 4.1)—should have only very small areas of sheet material left between the horns.

An alternative way to facilitate horn manufacturing for array receivers is to drill the horns with a custom shaped drill [77, 78]. Any horn profile that opens monotonically from throat to aperture is suitable for this technique. The transition from the circular horn to the rectangular waveguide, however, cannot be drilled and needs to be produced in a different process.

Casting as a replication process for feed horns has also been demonstrated around 100 GHz [79] and may be useful to produce feeds for array receivers.

4.3 Local Oscillators (LO) and LO Distribution

The local oscillator provides the reference frequency to downconvert the terahertz signal into a more accessible frequency range. Since the spectral line width of the LO ultimately limits the spectral resolution of the instrument, the LO has to be highly monochromatic. Typically, a spectral purity of $\Delta\nu/\nu < 10^{-7}$ is required for astronomical applications to allow resolving Doppler shifts down to < 0.1 km/s.

The exact amount of LO power required depends on the type of mixer and on the LO coupling technique. Superconducting mixers (SIS or HEB) usually need on the

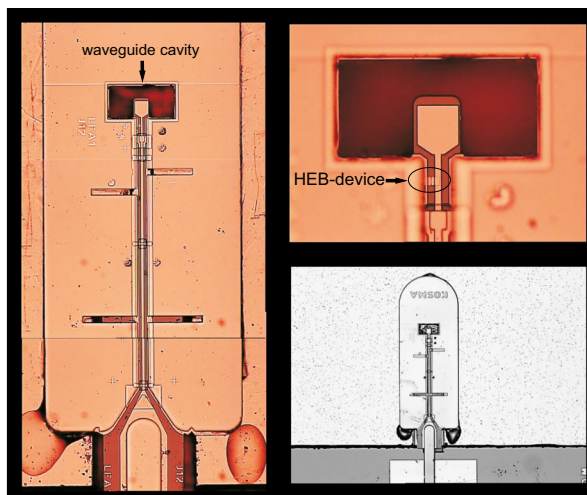


Fig. 6 1.9 THz waveguide HEB mixer device mounted in the copper waveguide ($96 \times 48 \mu\text{m}^2$) block with a $26 \mu\text{m}$ deep waveguide cavity (left hand picture). The top right magnifies the waveguide part and the HEB device, which sits on a $2 \mu\text{m}$ thick Si substrate surrounded by beam leads used for electrical contacts and for the registration of the device on the block. The bottom right shows a complete device with the IF connection to the circuit board's $100 \mu\text{m}$ wide line

order of $1 \mu\text{W}$ per pixel. To reduce cost and complexity of a receiver, it is in general desirable to use as few LO units as possible, which creates the need for high power monochromatic terahertz sources to serve as local oscillators in array receivers.

4.3.1 LO Sources

Frequency Multiplied Sources The classical local oscillator source today is a microwave synthesizer—typically operating around 10 GHz—followed by a series of power amplifiers and frequency multipliers. Due to the lack of amplifiers at frequencies beyond approximately 100 GHz, the power output of these chains is dictated by the efficiency of the subsequent frequency multiplication steps. Suitable commercial units provide a few tens of milliwatts at 100 GHz and drop by ≈ 2 dB per 100 GHz [80], where, to a certain extent, bandwidth can be traded for power. Power as high as $60 \mu\text{W}$ at 1900 GHz have been demonstrated [81].

While these power outputs are sufficient to operate even a large format array at wavelengths around 1 mm [21], at frequencies beyond 1 THz, it is increasingly difficult to feed even a modest size array [82].

At high multiplication factors, frequency multiplied sources may suffer from excess noise created by the amplification of phase noise in the multiplication process⁷, deteriorating the performance of the receiver. Careful choice of components like source synthesizers and amplifiers can reduce the LO noise. Interferometric diplexers (Section 4.3.2) also act as LO noise filters and help cleaning the LO signal. The best results are obtained with balanced mixers (Section 4.2), which intrinsically suppress LO noise [53].

Quantum Cascade Lasers A highly promising possible alternative LO source for higher frequencies is the quantum cascade laser (QCL) [83]. In contrast to frequency-multiplied sources, QCL output power tends to *increase* with higher frequencies. Already in the low terahertz regime, it reaches the milliwatt range, making QCLs extremely attractive for large format array receivers at frequencies beyond 1–2 THz.

To achieve the narrow line widths required for high resolution spectroscopy in astronomy, the lasers can be built as distributed feedback (DFB) devices, which, intrinsically, produce a highly monochromatic output [84]. In turn, however, the tunability of DFB lasers is very limited.

Better frequency control of the laser emission can be obtained by locking its frequency [85–87] or phase [88–90] to a suitable reference. Relative linewidths of 10^{-10} and below have been demonstrated by several groups.

Beyond the inconvenience that QCLs require cryogenic cooling, their widespread application as terahertz local oscillators is still impeded by the problem to achieve wide continuous frequency tuning and by their poor beam patterns. Both topics are actively being worked on and may be resolved in the near future.

⁷For a multiplication factor of N the phase noise rises by $20 \times \log N$

Photonic LOs Monochromatic terahertz radiation can also be produced by difference frequency generation. Two high power near-IR lasers are combined on a suitable photomixer, which emits the beat frequency. This technique has been demonstrated as LO in submillimeter heterodyne receivers [91]. A particular advantage is the very wide tuning range of the radiated frequency, allowing near octave bandwidth operation in a single device [92]. Beyond the instrumental complexity of these sources, their main drawback is—similar to frequency multiplied sources—their power roll-off at frequencies above 1 THz [93].

This technique is also used to optically create and distribute the local oscillator reference signals for the ALMA receivers [94].

4.3.2 LO Distribution

Up to about 0.5 THz, it is common to use waveguide couplers to couple the local oscillator power to the mixers. Due to the difficulties of manufacturing the small waveguide structures, higher frequency arrays today mostly couple the local oscillator (LO) signal to the mixers by means of optical diplexers. In the simplest case, this may just be a beam splitter, but in general will be an interferometric diplexer, which uses the limited LO power much more efficiently. The higher efficiency is paid for by a limited bandwidth: the 3 dB transmission bandwidth of a Martin–Puplett interferometer (MPI) is equal to its IF center frequency. A larger relative bandwidth can, in principle, be achieved with a Fabry–Perot interferometer (FPI) [49], but at the cost of decreased LO coupling efficiency and a very challenging optical alignment. Manufacturing tolerances and alignment difficulties also limit the usability of the MPI as today’s de-facto standard to modest array sizes [95].

LO coupling diplexers become obsolete if balanced mixers are used (Section 4.2), which have two separate input ports for the LO and the sky signal.

Before coupling the LO signal to the mixers, it has to be divided into individual signal channels to be distributed to the mixers. At lower frequencies, this splitting can also be done by waveguide couplers [21, 30]. At higher frequencies, it can be achieved by a succession of beam splitters, which extract appropriate fractions of power from the LO beam [20] or by a phase grating. Originally designed as Dammann gratings [15, 96], the preferred grating type soon became the Fourier grating [19, 97].

A grating, as a periodic modulation of either amplitude or phase of the incident field, produces a series of equally spaced diffraction orders. The relative intensity of these diffraction orders is set by the details of the modulation pattern of the grating unit cell⁸. Depending on the mixer arrangement, the unit cell can usually be tailored to equally distribute $\gtrsim 90\%$ of the incident power between those diffraction orders that match the mixer array geometry. Thus, the LO distribution at the grating is an image of the signal beam distribution at the telescope and can easily be reimaged to match the latter in the mixer plane.

⁸The far-field envelope of the diffraction orders is given by the Fourier transform of the unit cell field.

In a Fourier grating, the phase modulation of the unit cell is modeled as a Fourier series with a relatively small number of Fourier coefficients. This yields a smooth phase variation without discontinuities, which can be machined with high precision into a metallic surface to act as a reflection grating. Due to the smoothness of the surface, two-dimensional dispersion is easier to achieve than with Dammann gratings. In addition, the phase active surface can be projected and machined directly into a parabolic mirror, which in situ creates the planar phase front required for the grating, without the need for additional reimaging optics [98].

4.4 IF-processing and Backends

After downconversion in the mixers, the signal is amplified by cryogenic ultra-low noise amplifiers. Modern LNAs are available with bandwidths up to around 20 GHz and noise temperatures well below 10 K [99–101].

The LNA's power dissipation is a few milliwatts per pixel. For arrays with a large pixel count, this dissipation, together with the heat conduction through the IF output lines, drives the cooling needs of the instrument. In addition, the LNA input has to be well enough thermally insulated to not heat the mixers. To reduce the heat conduction through the IF output lines, conventional coaxial cables may be replaced by lower conductivity designs [102].

Additional room temperature amplification and possibly frequency conversion is commonly required for each pixel before feeding the signal into the spectroscopic backend. Although this only uses conventional high frequency electronics, it may be advantageous to invest in a lean and compact design to reduce cost, weight, volume and power consumption of the receiver.

The last element in the data acquisition process is the backend spectrometer, an array of filters followed by detectors that split the incoming signal band into many—typically several thousand—narrow spectral bins and detect the power in each bin. The direct implementation of this concept in filter banks is too clumsy for practical use. The dominating spectrometers over the last three decades have been acousto-optical spectrometers (AOS) [103] and digital correlators [104], both used in heterodyne arrays [15, 16, 20, 30].

Over the past 10 years, FPGA-based digital Fourier transform spectrometers (DFTS) emerged as the new standard spectrometer technology for heterodyne instruments [105–107]. Their good performance, ease of use and modest price also makes them the backend of choice for most modern array receivers [19, 21]. DFTSs use fast analog to digital converters (ADCs) to sample the IF signal amplitude at a very high rate. The FPGA pipes the data stream in real time through a fast Fourier transform algorithm and integrates the spectral data. The IF bandwidth coverable with DFTSs is limited by the speed of the ADC samplers. Bandwidths have been increasing steadily over the past years and are now approaching 5 GHz (Fig. 7).

The currently available bandwidth of 4 GHz covers a Doppler velocity range of approximately 2500 km/s at 0.5 THz at a resolution of 0.02 km/s, which is very comfortable for the vast majority of astronomical applications. At higher frequencies, the velocity range covered decreases proportionally to the observing wavelength,

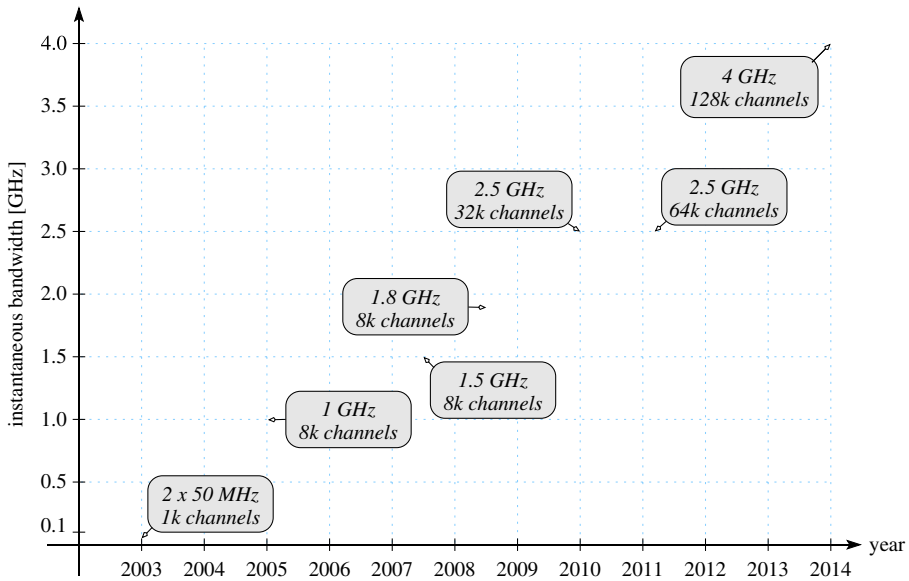


Fig. 7 Development of channel count and bandwidth of the MPIfR–developed digital Fourier transform spectrometers over the last decade (B. Klein, priv. comm.)

reaching 250 km/s at 5 THz. This is marginal for sources with wide spectral lines like for instance external galaxies seen edge-on. However, in practice, the more severe limitations arise from the limited bandwidth of the HEB mixers used at these frequencies (Section 4.2.2).

In a sideband separating receiver, DFTs may take over the function of the IF-hybrid, thereby simplifying the mixer hardware [108]. The IF-hybrid functionality is implemented digitally by a properly phased sampling and combination of the output signals of the two mixers.

4.5 System Aspects

Cryogenics All active array receivers use closed cycle refrigerators to produce the low temperatures needed for the superconducting detectors. Modern cryocoolers provide about 1 W of cooling power at 4.2 K. A significant fraction of this cooling capacity is required to remove the heat dissipated by the cryogenic low-noise amplifiers (~ 10 mW per pixel). For arrays with high pixel count, it may be necessary to combine two or more refrigerators. Although the cooling capacity of Gifford–McMahon refrigerators is somewhat large, most newer designs prefer pulse tube coolers, which have a much lower vibration level.

Electronics The control electronics for a large array can be very complex. Reducing this complexity to a minimum is an important design goal, when building an

instrument. In a single pixel SIS receiver, the mixer is usually connected by six or seven wires. This approach becomes impractical, when a large pixel count would require hundreds or thousands of cryogenic wire connections. Therefore, intelligent schemes of co-using wire, e.g., by applying the same bias voltage to all mixers, have to be employed for large arrays.

The bias control electronics can be simplified by using programmable components like microcontrollers or FPGAs, thereby shifting the complexity from hardware to software. A complex analog bias board can be replaced by a small board with a microcontroller and few peripheral components like ADCs and DACs. Such an intelligent board is more powerful, versatile, and can be multiplied more easily than a conventional analog board.

Receiver Tuning Manual receiver tuning is possible for moderate size arrays, but far too inefficient for large instruments. Automatic tuning algorithms have to be implemented [109]. Microcontroller-based bias electronics, as discussed above, makes it possible to parallelize the mixer tuning to minimize the receiver setup time when retuning a large array.

5 Summary

We have reviewed the development of heterodyne array receivers for astronomical application in the submillimeter and terahertz spectral range. We presented the underlying optics concepts and the technological milestones that make these instruments possible.

After a first series of array receivers deployed some 10 to 15 years ago, we are now standing at the threshold of the second generation with instruments with much higher pixel count, like SuperCam or the CHAI project for the proposed CCAT telescope and with the first true terahertz arrays like upGREAT.

Appendix: Optics

The optical system may be described in terms of ABCD transfer matrices, which cover both geometrical ray tracing and Gaussian beam propagation. The imaging condition of Section 4.1 requires the transfer matrix to be diagonal:

$$T = \begin{pmatrix} A & B \\ C & D \end{pmatrix} \quad \text{with} \quad B = C = 0 \quad \text{and} \quad A = 1/D = -M, \quad (5)$$

where the magnification M is the scaling factor for the beam spacing in geometrical optics and for the waist sizes in Gaussian optics [110].

If we consider a system of two phase transformers (lenses or mirrors) spaced by the sum of their focal lengths $F = f_1 + f_2$, the complete transfer matrix is

$$\begin{aligned}
 T &= \begin{pmatrix} 1 & d_{\text{out}} \\ 0 & 1 \end{pmatrix} \begin{pmatrix} 1 & 0 \\ -1/f_2 & 1 \end{pmatrix} \begin{pmatrix} 1 & F \\ 0 & 1 \end{pmatrix} \begin{pmatrix} 1 & 0 \\ -1/f_1 & 1 \end{pmatrix} \begin{pmatrix} 1 & d_{\text{in}} \\ 0 & 1 \end{pmatrix} \\
 &= \begin{pmatrix} 1 & d_{\text{out}} \\ 0 & 1 \end{pmatrix} \begin{pmatrix} -M & F \\ 0 & -1/M \end{pmatrix} \begin{pmatrix} 1 & d_{\text{in}} \\ 0 & 1 \end{pmatrix} \\
 &= \begin{pmatrix} -M & F - Md_{\text{in}} - d_{\text{out}}/M \\ 0 & -1/M \end{pmatrix}, \tag{6}
 \end{aligned}$$

where d_{in} and d_{out} are the input and output distances, respectively, and $M = f_2/f_1$ is the magnification of the system. We obtain the result of Eq. 4 if we turn T into a diagonal matrix by setting

$$F - Md_{\text{in}} - \frac{d_{\text{out}}}{M} = 0 \quad \Rightarrow \quad d_{\text{out}} = MF - M^2d_{\text{in}}. \tag{7}$$

Obviously, $d_{\text{in}} = f_1$ implies $d_{\text{out}} = f_2$.

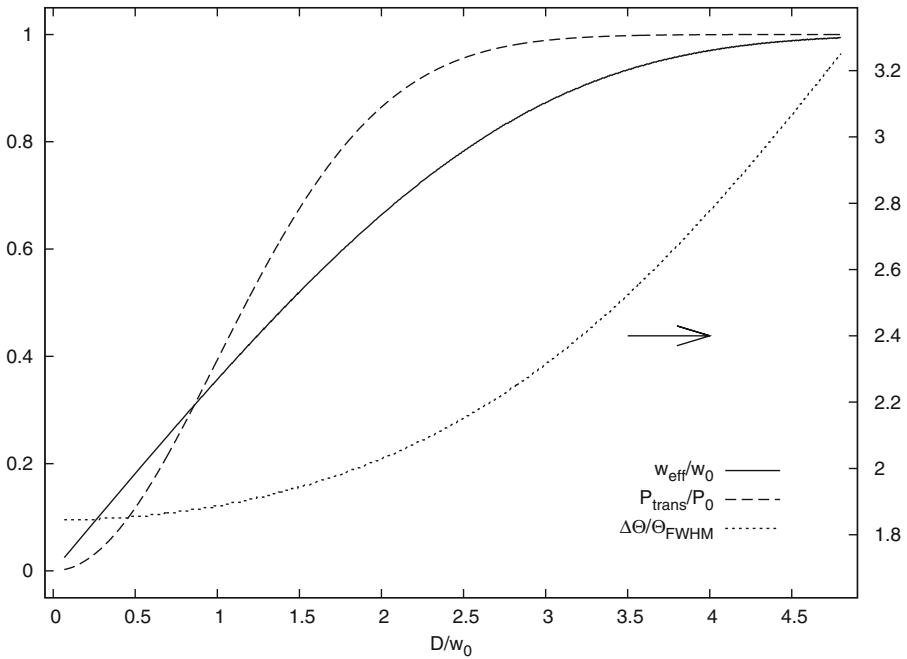


Fig. 8 Effective beam waist w_{eff} produced by diffraction, if a Gaussian beam of waist w_0 is truncated by a circular aperture of diameter D (solid line). The dashed line gives the relative power transmitted through this aperture. Using Eq. 3 with $s_M/w_M = D/w_{\text{eff}}$ and $T_E = 14$ dB yields the dotted curve, which shows that beam spacing can only be pushed under $2 \times \theta_{\text{FWHM}}$ if severe truncation losses are accepted

Figure 8 illustrates how truncation affects a Gaussian beam. For apertures of diameter $D > 3w_0$, the effective beam waist size w_{eff} approaches the unvignetted waist size w_0 , whereas in the limit of very small apertures, the beam waist is entirely dominated by the aperture diameter: $w_{\text{eff}} \approx 0.36 \times D$, independent of w_0 . Similarly, the power loss due to the truncation increases rapidly for smaller apertures. Thus, the packing density of the beams on the sky is ultimately limited to $0.18\sqrt{T_E}/0.36 = \sqrt{T_E}/2$ (Eq. 3), and in practice, values lower than $\Delta\Theta < 2\Theta_{\text{FWHM}}$ would seriously compromise the sensitivity of the instrument.

References

1. L.A. Samoska, IEEE Transactions on Terahertz Science and Technology **1**(1), 9 (2011)
2. W. Deal, X.B. Mei, K.M.K.H. Leong, V. Radisic, S. Sarkozy, R. Lai, IEEE Transactions on Terahertz Science and Technology **1**(1), 25 (2011)
3. T. Phillips, D. Woody, G. Dolan, R. Miller, R. Linke, IEEE Transactions on Magnetics **17**(1), 684 (1981)
4. A.R. Kerr, M.J. Feldman, S.K. Pan, in *Proceedings of the 8th International Symposium on Space Terahertz Technology* (Cambridge, 1997), pp. 101–111
5. T. de Graauw, in *2011 36th International Conference on Infrared, Millimeter and Terahertz Waves (IRMMW-THz)* (2011), pp. 1–4
6. S. Claude, P. Niranjana, F. Jiang, D. Duncan, D. Garcia, M. Halman, H. Ma, I. Wevers, K. Yeung, Journal of Infrared, Millimeter, and Terahertz Waves **35**(6-7), 563 (2014)
7. S. Asayama, T. Takahashi, K. Kubo, T. Ito, M. Inata, T. Suzuki, T. Wada, T. Soga, C. Kamada, M. Karatsu, Y. Fujii, Y. Obuchi, S. Kawashima, H. Iwashita, Y. Uzawa, Publications of the Astronomical Society of Japan **66**(3) (2014)
8. A. Kerr, S.K. Pan, S. Claude, P. Dindo, A. Lichtenberger, J. Efland, E. Lauria, IEEE Transactions on Terahertz Science and Technology **4**(2), 201 (2014)
9. S. Mahieu, D. Maier, B. Lazareff, A. Navarrini, G. Celestin, J. Chalain, D. Geoffroy, F. Laslaz, G. Perrin, IEEE Transactions on Terahertz Science and Technology **2**(1), 29 (2012)
10. T. Tamura, T. Noguchi, Y. Sekimoto, W. Shan, N. Sato, Y. Iizuka, K. Kumagai, Y. Niizeki, M. Iwakuni, T. Ito, IEEE Transactions on Applied Superconductivity **25**(3), 1 (2015)
11. B.D. Jackson, R. Hesper, J. Adema, J. Barkhof, A.M. Baryshev, T. Zijlstra, S. Zhu, T.M. Klapwijk, in *Twentieth International Symposium on Space Terahertz Technology*, ed. by E. Bryerton, A. Kerr, A. Lichtenberger (2009), pp. 7–11
12. A. Gonzalez, Y. Fujii, K. Kaneko, M. Kroug, T. Kojima, K. Kuroiwa, A. Miyachi, K. Makise, Z. Wang, S. Asayama, Y. Uzawa, in *Millimeter, Submillimeter, and Far-Infrared Detectors and Instrumentation for Astronomy VII*, vol. 9153, ed. by W.S. Holland, J. Zmuidzinas (2014), vol. 9153, pp. 91,530N–91,530N–13
13. Pütz, P., Honingh, C. E., Jacobs, K., Justen, M., Schultz, M., Stutzki, J., Astronomy and Astrophysics **542**, L2 (2012)
14. D. Büchel, P. Pütz, K. Jacobs, M. Schultz, U.U. Graf, C. Risacher, H. Richter, O. Ricken, H.W. Hübers, R. Güsten, C.E. Honingh, J. Stutzki, IEEE Transactions on Terahertz Science and Technology **5**(2), 207 (2015)
15. R. Güsten, G. Ediss, F. Gueth, K. Gundlach, H. Hauschildt, C. Kasemann, T. Klein, J. Kooi, A. Korn, I. Krämer, R. LeDuc, H. Mattes, K. Meyer, E. Perchtold, M. Pilz, R. Sacher, M. Scherschel, P. Schilke, G. Schneider, J. Schraml, D. Skaley, R. Stark, W. Wetzker, H. Wiedenhöfer, S. Wongsowijoto, F. Wyrowski, in *Advanced Technology MMW, Radio, and Terahertz Telescopes*, ed. by T.G. Phillips (Proceedings of SPIE Vol. 3357, 1998)
16. U.U. Graf, S. Heyminck, E.A. Michael, S. Stanko, C.E. Honingh, K. Jacobs, R.T. Schieder, J. Stutzki, B. Vowinkel, in *Millimeter and Submillimeter Detectors for Astronomy, Proceedings of the SPIE*, vol. 4855, ed. by T.G. Phillips, J. Zmuidzinas (2003), *Proceedings of the SPIE*, vol. 4855, pp. 322–329

17. C. Walker, C. Groppi, D. Golish, C. Kulesa, A. Hungerford, C. Drouët d'Aubigny, K. Jacobs, U. Graf, C. Martin, J. Kooi, in *Proceedings of the 12th International Symposium on Space Terahertz Technology*, ed. by I. Mehdi (JPL Publication 01–18, San Diego, 2001), pp. 540–552
18. C.E. Groppi, C.K. Walker, C. Kulesa, D. Golish, A. Hedden, G. Narayanan, A.W. Lichtenberger, J.W. Kooi, U.U. Graf, S. Heyminck, in *Millimeter and Submillimeter Detectors for Astronomy II*, vol. 5498, ed. by C.M. Bradford, P.A.R. Ade, J.E. Aguirre, J.J. Bock, M. Dragovan, L. Duband, L. Earle, J. Glenn, H. Matsuhara, B.J. Naylor, H.T. Nguyen, M. Yun, J. Zmuidzinas (2004), vol. 5498, pp. 290–299
19. C. Kasemann, R. Güsten, S. Heyminck, B. Klein, T. Klein, S.D. Philipp, A. Korn, G. Schneider, A. Henseler, A. Baryshev, T.M. Klapwijk, in *Millimeter and Submillimeter Detectors and Instrumentation for Astronomy III, Society of Photo-Optical Instrumentation Engineers (SPIE) Conference Series*, vol. 6275, ed. by Z. J., W.S. Holland, S. Withington, W.D. Duncan (2006), *Society of Photo-Optical Instrumentation Engineers (SPIE) Conference Series*, vol. 6275
20. J.V. Buckle, R.E. Hills, H. Smith, W.R.F. Dent, G. Bell, E.I. Curtis, R. Dace, H. Gibson, S.F. Graves, J. Leech, J.S. Richer, R. Williamson, S. Withington, G. Yassin, R. Bennett, P. Hastings, I. Laidlaw, J.F. Lightfoot, T. Burgess, P.E. Dewdney, G. Hovey, A.G. Willis, R. Redman, B. Wooff, D.S. Berry, B. Cavanagh, G.R. Davis, J. Dempsey, P. Friberg, T. Jenness, R. Kackley, N.P. Rees, R. Tilanus, C. Walther, W. Zwart, T.M. Klapwijk, M. Kroug, T. Zijlstra, *Monthly Notices of the Royal Astronomical Society* **399**(2), 1026 (2009)
21. C. Groppi, C. Walker, C. Kulesa, D. Golish, J. Kloosterman, S. Weinreb, G. Jones, J. Barden, H. Mani, T. Kuiper, J. Kooi, A. Lichtenberger, T. Cecil, G. Narayanan, P. Pütz, A. Hedden, in *Proceedings of the 20th International Symposium on Space Terahertz Technology* (Charlottesville, 2009), pp. 90–96
22. G.L. Pilbratt, J.R. Riedinger, T. Passvogel, G. Crone, D. Doyle, U. Gageur, A.M. Heras, C. Jewell, L. Metcalfe, S. Ott, M. Schmidt, *Astronomy and Astrophysics* **518**, L1 (2010)
23. C. Walker, C. Kulesa, P. Bernasconi, H. Eaton, N. Rolander, C. Groppi, J. Kloosterman, T. Cottam, D. Lesser, C. Martin, A. Stark, D. Neufeld, C. Lisse, D. Hollenbach, J. Kawamura, P. Goldsmith, W. Langer, H. Yorke, J. Sterne, A. Skalare, I. Mehdi, S. Weinreb, J. Kooi, J. Stutzki, U. Graf, M. Brasse, C. Honingh, R. Simon, M. Akylmaz, P. Pütz, M. Wolfire, in *Society of Photo-Optical Instrumentation Engineers (SPIE) Conference Series*, vol. 7733 (2010), vol. 7733
24. E.T. Young, E.E. Becklin, P.M. Marcum, T.L. Roellig, J.M.D. Buizer, T.L. Herter, R. Güsten, E.W. Dunham, P. Temi, B.G. Andersson, D. Backman, M. Burgdorf, L.J. Caroff, S.C. Casey, J.A. Davidson, E.F. Erickson, R.D. Gehrz, D.A. Harper, P.M. Harvey, L.A. Helton, S.D. Horner, C.D. Howard, R. Klein, A. Krabbe, I.S. McLean, A.W. Meyer, J.W. Miles, M.R. Morris, W.T. Reach, J. Rho, M.J. Richter, H.P. Röser, G. Sandell, R. Sankrit, M.L. Savage, E.C. Smith, R.Y. Shuping, W.D. Vacca, J.E. Vaillancourt, J. Wolf, H. Zinnecker, *The Astrophysical Journal Letters* **749**(2), L17 (2012)
25. S. Heyminck, U.U. Graf, R. Güsten, J. Stutzki, H.W. Hübers, P. Hartogh, *Astronomy and Astrophysics* **542**, L1 (2012)
26. J.M. Payne, *Review of Scientific Instruments* **59**(9), 1911 (1988)
27. C. Groppi, J. Kawamura, *IEEE Transactions on Terahertz Science and Technology* **1**(1), 85 (2011)
28. T.G. Phillips, in *Bulletin of the American Astronomical Society, Bulletin of the American Astronomical Society*, vol. 20 (1988), *Bulletin of the American Astronomical Society*, vol. 20, p. 690
29. R. Güsten, L.Å. Nyman, P. Schilke, K. Menten, C. Cesarsky, R. Booth, *Astronomy and Astrophysics* **454**, L13 (2006)
30. K.F. Schuster, C. Boucher, W. Brunswig, M. Carter, J.Y. Chenu, B. Foullieux, A. Greve, D. John, B. Lazareff, S. Navarro, A. Perrigouard, J.L. Pollet, A. Sievers, C. Thum, H. Wiesemeyer, *Astronomy and Astrophysics* **423**, 1171 (2004)
31. J.W.M. Baars, B.G. Hooghoudt, P.G. Mezger, M.J. de Jonge, *Astronomy and Astrophysics* **175**, 319 (1987)
32. C.G. Degiacomi, R. Schieder, J. Stutzki, G. Winnewisser, *Optical Engineering* **34**(9) (1995)
33. Y. Fukui, T. Onishi, N. Mizuno, A. Mizuno, H. Ogawa, Y. Yonekura, J. Stutzki, U. Graf, C. Kramer, R. Simon, F. Bertoldi, U. Klein, F. Bensch, B.C. Koo, Y.S. Park, L. Bronfman, J. May, M. Burton, A. Benz, *IAU Special Session I*, 21 (2006)
34. R. Hills, B. Edwards, J. Hall, in *IEE Colloquium on Mechanical Aspects of Antenna Design* (1989), pp. 3/1–3/4
35. J.W.M. Baars, R.N. Martin, J.G. Mangum, J.P. McMullin, W.L. Peters, *Publications of the ASP* **111**, 627 (1999)

36. C. Risacher, R. Güsten, J. Stutzki, H.W. Hübers, P. Pütz, A. Bell, D. Büchel, I. Camara, R. Castenholz, M. Choi, U. Graf, S. Heyminck, C. Honingh, K. Jacobs, M. Justen, B. Klein, T. Klein, C. Leinz, N. Reyes, H. Richter, O. Ricken, A. Semenov, A. Wunsch, in *39th International Conference on Infrared, Millimeter, and Terahertz waves (IRMMW-THz)* (2014), pp. 1–2
37. A. Russell, H. van de Stadt, B. Hayward, B. Duncan, in *Multi-Feed Systems for Radio Telescopes, Astronomical Society of the Pacific Conference Series*, vol. 75, ed. by D.T. Emerson, J.M. Payne (1995), *Astronomical Society of the Pacific Conference Series*, vol. 75, p. 179
38. D. Allan, Proceedings of the IEEE **54**(2), 221 (1966)
39. G. Chattopadhyay, C. Lee, C. Jung, R. Lin, A. Peralta, I. Mehdi, N. Llombert, B. Thomas, in *IEEE International Symposium on Antennas and Propagation (APSURSI)* (2011), pp. 3007–3010
40. P.F. Goldsmith, *Quasioptical Systems* (IEEE Press, ISBN 0-7803-3439-6, 1998)
41. VDI Nominal Horn Specifications. http://www.vadiodes.com/images/AppNotes/vdi%20feedhorn%20summary%202011_10_31.pdf. Accessed: 2014-12-04
42. H.M. Pickett, J.C. Hardy, J. Farhoomand, IEEE Transactions on Microwave Theory and Techniques **32**(8), 936 (1984)
43. G. Cortes-Medellin, in *39th International Conference on Infrared, Millimeter, and Terahertz waves* (2014), pp. 1–2
44. T. Lüthi, D. Rabanus, U.U. Graf, C. Granet, A. Murk, Review of Scientific Instruments **77**, 4702 (2006)
45. A. Gatesman, J. Waldman, M. Ji, C. Musante, S. Yagvesson, Microwave and Guided Wave Letters, IEEE **10**(7), 264 (2000)
46. A. Wagner-Gentner, U.U. Graf, D. Rabanus, K. Jacobs, Infrared Physics and Technology **48**, 249 (2006)
47. R. Datta, C.D. Munson, M.D. Niemack, J.J. McMahon, J. Britton, E.J. Wollack, J. Beall, M.J. Devlin, J. Fowler, P. Gallardo, J. Hubmayr, K. Irwin, L. Newburgh, J.P. Nibarger, L. Page, M.A. Quijada, B.L. Schmitt, S.T. Staggs, R. Thornton, L. Zhang, Appl. Opt. **52**(36), 8747 (2013)
48. J. Ruze, Proceedings of the IEEE **54**(4), 633 (1966)
49. M. Brasse, Design, Aufbau, Test und Integration der Empfänger-Optik des Stratospheric Terahertz Observatory. Ph.D. thesis, Universität zu Köln (2014)
50. R. Kackley, D. Scott, E. Chapin, P. Friberg, in *Software and Cyberinfrastructure for Astronomy*, vol. 7740, ed. by N.M. Radziwill, A. Bridger (2010), vol. 7740
51. D. Bintley, W.S. Holland, M.J. MacIntosh, P. Friberg, G.S. Bell, D.A. Berke, D.S. Berry, R.M. Berthold, J.L. Cookson, I.M. Coulson, M.J. Currie, J.T. Dempsey, A.G. Gibb, B.H. Gorges, S.F. Graves, T. Jenness, D.I. Johnstone, H.A.L. Parsons, H.S. Thomas, C. Walther, J.G.A. Wouterloot, in *Millimeter, Submillimeter, and Far-Infrared Detectors and Instrumentation for Astronomy VII*, vol. 9153, ed. by W.S. Holland, J. Zmuidzinas (2014), vol. 9153, p. 3
52. J. Zmuidzinas, N.G. Ugras, D. Miller, M. Gaidis, H.G. LeDuc, J.A. Stern, IEEE Transactions on Applied Superconductivity **5**(2), 3053 (1995)
53. M.P. Westig, K. Jacobs, J. Stutzki, M. Schultz, M. Justen, C.E. Honingh, Superconductor Science and Technology **24**(8), 085012 (2011)
54. M.P. Westig, M. Justen, K. Jacobs, J. Stutzki, M. Schultz, F. Schomacker, N. Honingh, Journal of Applied Physics **112**(9), 093919 (2012)
55. Y. Serizawa, Y. Sekimoto, M. Kamikura, W. Shan, T. Ito, International Journal of Infrared and Millimeter Waves **29**(9), 846 (2008)
56. J.R. Tucker, M.J. Feldman, Rev. Mod. Phys. **57**, 1055 (1985)
57. A.V. Räisänen, W.R. McGrath, P.L. Richards, F.L. Lloyd, in *Microwave Symposium Digest, 1985 IEEE MTT-S International* (1985), pp. 669–672
58. A. Kerr, S.K. Pan, M. Feldman, International Journal of Infrared and Millimeter Waves **9**(2), 203 (1988)
59. K. Jacobs, U. Kotthaus, B. Vowinkel, International Journal of Infrared and Millimeter Waves **13**(1), 15 (1992)
60. B.D. Jackson, G. de Lange, T. Zijlstra, M. Kroug, T.M. Klapwijk, J.A. Stern, Journal of Applied Physics **97**(11), 113904 (2005)
61. Y. Uzawa, Y. Fujii, A. Gonzalez, K. Kaneko, M. Kroug, T. Kojima, A. Miyachi, K. Makise, S. Saito, H. Terai, Z. Wang, IEEE Transactions on Applied Superconductivity **PP**(99), 1 (2014)
62. E.M. Gershenzon, G.N. Gol'tsman, I.G. Gogidze, Y.P. Gusev, A.I. Elant'ev, B.S. Karasik, A.D. Semenov, Superconductivity **3**(10), 1582 (1990)

63. H. Ekström, B.S. Karasik, E.L. Kollberg, K.S. Yngvesson, *IEEE Transactions on Microwave Theory and Techniques* **43**(4), 938 (1995)
64. S. Bevilacqua, S. Cherednichenko, V. Drakinskiy, J. Stake, H. Shibata, Y. Tokura, *Applied Physics Letters* **100**(3), 033504 (2012)
65. D. Cunnane, J. Kawamura, M. Wolak, N. Acharya, T. Tan, X. Xi, B. Karasik, *IEEE Transactions on Applied Superconductivity* **25**(3), 1 (2015)
66. P. Khosropanah, J.R. Gao, W.M. Laauwen, M. Hajenius, T.M. Klapwijk, *Applied Physics Letters* **91**(22), 221111 (2007)
67. S. Cherednichenko, V. Drakinskiy, T. Berg, P. Khosropanah, E. Kollberg, *Review of Scientific Instruments* **79**(3), 034501 (2008)
68. W. Zhang, P. Khosropanah, J.R. Gao, T. Bansal, T.M. Klapwijk, W. Miao, S.C. Shi, *Journal of Applied Physics* **108**(9), 093102 (2010)
69. D. Meledin, A. Pavolotsky, V. Desmaris, I. Lapkin, C. Risacher, V. Perez, D. Henke, O. Nystrom, E. Sundin, D. Dochev, M. Pantaleev, M. Fredrixon, M. Strandberg, B. Voronov, G. Goltsman, V. Belitsky, *IEEE Transactions on Microwave Theory and Techniques* **57**(1), 89 (2009)
70. F. Boussaha, J. Kawamura, J. Stern, C. Jung-Kubiak, *IEEE Transactions on Terahertz Science and Technology* **4**(5), 545 (2014)
71. B. Thomas, *IEEE Transactions on Antennas and Propagation* **26**(2), 367 (1978)
72. R.J. Wylde, D.H. Martin, *IEEE Transactions on Microwave Theory and Techniques* **41**(10), 1691 (1993)
73. J.F. Johansson, N.D. Whyborn, *IEEE Transactions on Microwave Theory and Techniques* **40**(5), 795 (1992)
74. B.N. Ellison, M.L. Oldfield, B.J. Maddison, C.M. Mann, D.N. Matheson, A.F. Smith, in *Proceedings of the 5th International Symposium on Space Terahertz Technology* (Ann Arbor, 1994), pp. 851–860
75. C. Granet, G.L. James, R. Bolton, G. Moorey, *IEEE Transactions on Antennas and Propagation* **52**(3), 848 (2004)
76. R.W. Haas, D. Brest, H. Mueggenburg, L. Lang, D. Heimlich, *International Journal of Infrared and Millimeter Waves* **14**(11), 2289 (1993)
77. J. Leech, B.K. Tan, G. Yassin, P. Kittara, S. Wangsuya, J. Treuttel, M. Henry, M.L. Oldfield, P.G. Huggard, *Astronomy and Astrophysics* **532**, A61 (2011)
78. J. Leech, B.K. Tan, G. Yassin, P. Kittara, S. Wangsuya, *IEEE Transactions on Terahertz Science and Technology* **2**(1), 61 (2012)
79. J.M. Munier, A. Maestrini, M.C. Salez, M. Guillon, B. Marchand, in *Radio Telescopes*, vol. 4015, ed. by H.R. Butcher (Proc. SPIE, 2000), vol. 4015, pp. 500–514
80. VDI Amplifier/Multiplier Chains (AMCs). http://www.vadiodes.com/images/Products/AMCMixAMC/AMC_Brochure_2014_07.pdf. Accessed: 2014-12-04
81. I. Mehdi, J.V. Siles, A. Maestrini, R. Lin, C. Lee, E. Schlecht, G. Chattopadhyay, in *Millimeter, Submillimeter, and Far-Infrared Detectors and Instrumentation for Astronomy VI*, vol. 8452, ed. by W.S. Holland (2012), vol. 8452, pp. 845,212–845,212–6
82. J.V. Siles, C. Lee, R. Lin, E. Schlecht, G. Chattopadhyay, I. Mehdi, in *39th International Conference on Infrared, Millimeter, and Terahertz waves* (2014), pp. 1–3
83. J. Faist, F. Capasso, D.L. Sivco, C. Sirtori, A.L. Hutchinson, A.Y. Cho, *Science* **264**(5158), 553 (1994)
84. H.W. Hübers, in *39th International Conference on Infrared, Millimeter, and Terahertz waves* (2014)
85. A.L. Betz, R.T. Boreiko, B.S. Williams, S. Kumar, Q. Hu, J.L. Reno, *Opt. Lett.* **30**(14), 1837 (2005)
86. H. Richter, S. Pavlov, A. Semenov, L. Mahler, A. Tredicucci, H. Beere, D. Ritchie, H.W. Hübers, *Applied Physics Letters* **96**(7), 071112 (2010)
87. Y. Ren, J.N. Hovenier, M. Cui, D.J. Hayton, J.R. Gao, T.M. Klapwijk, S.C. Shi, T.Y. Kao, Q. Hu, J.L. Reno, *Applied Physics Letters* **100**(4), 041111 (2012)
88. D. Rabanus, U.U. Graf, M. Philipp, O. Ricken, J. Stutzki, B. Vowinkel, M.C. Wiedner, C. Walther, M. Fischer, J. Faist, *Optics Express* **17**, 1159 (2009)
89. P. Khosropanah, A. Baryshev, W. Zhang, W. Jellema, J.N. Hovenier, J.R. Gao, T.M. Klapwijk, D.G. Paveliev, B.S. Williams, S. Kumar, Q. Hu, J.L. Reno, B. Klein, J.L. Hesler, *Opt. Lett.* **34**(19), 2958 (2009)
90. M. Ravaro, C. Manquest, C. Sirtori, S. Barbieri, G. Santarelli, K. Blary, J.F. Lampin, S.P. Khanna, E.H. Linfield, *Opt. Lett.* **36**(20), 3969 (2011)
91. I. Cámara Mayorga, P. Muñoz Pradas, E.A. Michael, M. Mikulics, A. Schmitz, P. van der Wal, C. Kasemann, R. Güsten, K. Jacobs, M. Marso, H. Lüth, P. Kordoš, *Journal of Applied Physics* **100**(4), 043116 (2006)

92. S. Kohjiro, K. Kikuchi, M. Maezawa, T. Furuta, A. Wakatsuki, H. Ito, N. Shimizu, T. Nagatsuma, Y. Kado, *Applied Physics Letters* **93**(9), 093508 (2008)
93. I. Cámara Mayorga, E.A. Michael, A. Schmitz, P. van der Wal, R. Güsten, K. Maier, A. Dewald, *Applied Physics Letters* **91**(3), 031107 (2007)
94. B. Shillue, W. Grammer, C. Jacques, R. Brito, J. Meadows, J. Castro, Y. Masui, R. Treacy, J.F. Cliche, in *Millimeter, Submillimeter, and Far-Infrared Detectors and Instrumentation for Astronomy VI*, vol. 8452, ed. by W.S. Holland (2012), vol. 8452, pp. 845,216–845,216–6
95. M. Kotiranta, C. Leinz, T. Klein, V. Krozer, H.J. Wunsch, *Journal of Infrared, Millimeter, and Terahertz Waves* **33**(11), 1138 (2012)
96. H. Dammann, E. Klotz, *Optica Acta* **24** (1977)
97. U.U. Graf, S. Heyminck, *IEEE Transactions on Antennas and Propagation* **49**, 542 (2001)
98. S. Heyminck, U.U. Graf, in *Proceedings of the 12th International Symposium on Space Terahertz Technology*, ed. by I. Mehdi (JPL Publication 01–18, San Diego, 2001), pp. 563–570
99. S. Weinreb, J.C. Bardin, H. Mani, *IEEE Transactions on Microwave Theory and Techniques* **55**(11) (2007)
100. G. Schlee, J. Alestig, J. Halonen, A. Malmros, B. Nilsson, P. Nilsson, J. Starski, N. Wadefalk, H. Zirath, J. Grahn, *IEEE Electron Device Letters* **33**(5), 664 (2012)
101. Low Noise Factory. <http://www.lownoisefactory.com>. Accessed: 2015-03-31
102. A.I. Harris, M. Sieth, J.M. Lau, S.E. Church, L.A. Samoska, K. Cleary, *Review of Scientific Instruments* **83**(8), 086105 (2012)
103. J. Horn, O. Siebertz, F. Schmülling, C. Kunz, R. Schieder, G. Winnewisser, *Exper. Astron.* **9**(1), 17 (1999)
104. R.P. Escoffier, G. Comoretto, J.C. Webber, A. Baudry, C.M. Broadwell, J.H. Greenberg, R.R. Treacy, P. Cais, B. Quertier, P. Camino, A. Bos, A.W. Gunst, *Astronomy and Astrophysics* **462**, 801 (2007)
105. A.O. Benz, P.C. Grigis, V. Hungerbühler, H. Meyer, C. Monstein, B. Stuber, D. Zardet, *Astronomy and Astrophysics* **442**, 767 (2005)
106. M. Krus, J. Embretsén, A. Emrich, S. Back-Andersson, in *Proceedings of the 22nd International Symposium on Space Terahertz Technology* (Tucson, 2011)
107. B. Klein, S. Hochgürtel, I. Krämer, A. Bell, K. Meyer, R. Güsten, *Astronomy and Astrophysics* **542**, L3 (2012)
108. R. Rodríguez, R. Finger, F.P. Mena, N. Reyes, E. Michael, L. Bronfman, *Publications of the ASP* **126**, 380 (2014)
109. S. Stanko, U.U. Graf, S. Heyminck, in *Proceedings of the 13th International Symposium on Space Terahertz Technology*, ed. by R. Blundell, E. Tong (Harvard University, Cambridge, 2002)
110. D.H. Martin, J.W. Bowen, *IEEE Transactions on Microwave Theory and Techniques* **41**(10), 1676 (1993)